LYMPHOID NEOPLASIA

LMP1 mediates multinuclearity through downregulation of shelterin proteins and formation of telomeric aggregates

Valérie Lajoie,[1,2] Bruno Lemieux,[1,2] Bassem Sawan,[3] Daniel Lichtensztejn,[4] Zelda Lichtensztejn,[4] Raymund Wellinger,[2] Sabine Mai,[4] and Hans Knecht[1,2,5]

[1]Divison d'Hématologie, Département de Médecine, [2]Département de Microbiologie/Infectiologie, and [3]Département de Pathologie, Centre Hospitalier Universitaire de Sherbrooke, Université de Sherbrooke, Sherbrooke, QC, Canada; [4]Manitoba Institute of Cell Biology, University of Manitoba, Winnipeg, MB, Canada; and [5]Jewish General Hospital, McGill University, Montréal, QC, Canada

Key Points

- LMP1 expression in post germinal center B cells results in downregulation of shelterin proteins, telomeric aggregates, and multinuclearity.
- LMP1 targets TRF1, TRF2, and POT1 reversibly at the transcriptional/translational level, and TRF2 is essential to block multinuclearity.

Hodgkin lymphoma (HL) and Burkitt lymphoma are both germinal center–derived B-cell lymphomas. To assess the consequences of permanent latent membrane protein 1 (LMP1) expression as observed in tumor cells of Epstein-Barr virus (EBV) –associated HL, we analyzed 3-dimensional (3D) telomere dynamics and measured the expression of shelterin proteins at the transcriptional and translational level and their topographic distribution in the EBV-negative Burkitt cell line BJAB stably transfected with an inducible LMP1 system. Stable LMP1 expression led to a highly significant increase of multinucleated cells, nuclear volume, and 3D telomeric aggregates when compared with the LMP1-suppressed BJAB controls. Most importantly, LMP1 induced a significant downregulation of the shelterin components TRF1, TRF2, and POT1 at the transcriptional and translational level, and this downregulation was reversed after resuppression of LMP1. In addition, as revealed by spectral karyotyping, LMP1 induced "outré" giant cells and hypoploid "ghost" cells. This LMP1-induced multinucleation was blocked upon LMP1-independent TRF2 expression. These results show that LMP1-dependent deregulation of telomere stability and nuclear organization via shelterin downregulation, in particular TRF2, favors chromosomal rearrangements. We speculate that telomeric aggregates and ongoing breakage-bridge-fusion cycles lead to disturbed cytokinesis and finally to multinuclearity, as observed in EBV-associated HL. (*Blood*. 2015;125(13):2101-2110)

Introduction

The binuclear or multinuclear Reed-Sternberg (RS) cells, the diagnostic element of Hodgkin lymphoma (HL), originate from mononuclear precursors called Hodgkin (H) cells via endoreplication and have a limited capacity to divide further.[1,2] RS cells still contribute to the pathogenesis through autocrine stimulation of H cells[3] and cytokine-induced B symptoms (reviewed in Khan[4]). H and RS cells are derived from germinal center B cells,[5] and circulating monoclonal B cells have been identified as putative precursors of H cells.[6] Three-dimensional (3D) quantitative fluorescence in situ hybridization (qFISH), a technique for visualizing telomeres,[7] showed in cultured cells and biopsies that RS cells are true end-stage tumor cells.[8] The number of nuclei in RS cells correlates closely with the 3D organization of telomeres, and we speculated that further nuclear divisions become impossible because of sustained telomere shortening, loss, and aggregation and formation of "ghost" nuclei in which many chromosomes lack terminal repeat sequences. These phenomena were identified in both classical Epstein-Barr virus (EBV) –negative and EBV-positive HL.[9]

In EBV-positive HL, the H and RS cells express the EBV-encoded latent membrane protein 1 (LMP1)[10] or its deletion variants.[11]

Presentation, clinical course, and response to chemotherapy for EBV-associated HL are very similar to those in EBV-negative HL,[12] but the LMP1-expressing nodular sclerosis type may have a less favorable long-term prognosis,[13,14] and relevant differences in EBV association are observed according to socioeconomic status.[15] The risk of developing LMP1-expressing HL within a median incubation time of 4 years after symptomatic EBV infection is significantly increased,[16] but the reason for this remains unclear. In symptomatic mononucleosis infectiosa, multinucleated RS-like cells may occur, but these cells are polyclonal and exhibit CD15⁻ and, most importantly, they always express the B-cell–specific transcription factors BOB.1 and OCT-2, which are absent in true RS cells.[17]

Our recent observations document that very short telomeres are a hallmark of LMP1-expressing RS cells, even in young patients.[18] Short-term cultures of ex vivo EBV-infected normal human B lymphocytes show partial displacement of the telomeric protein TRF2, which is associated with a high level of nonclonal structural aberrations, namely Robertsonian translocations, unbalanced translocations, and chromatid gaps.[19] Furthermore, the EBV nuclear

antigen-1 (EBNA1) induces loss or gain of telomere signals and promotes telomere fusion.[20] Finally, RS cells contain giant "zebra" chromosomes as a result of multiple breakage-bridge-fusion cycles.[21] These results are consistent with the hypothesis that EBV interacts with the shelterin-telomere complex and that the oncoprotein LMP1 directly or indirectly targets key proteins of it, and by doing so, initiates 3D telomere–related changes in germinal center–derived B cells favoring the formation of H and RS cells.

To test this hypothesis, we used a long-term tet-off inducible LMP1 expression system in stable transfectants of BJAB cells.[22] BJAB is an EBV-negative African Burkitt lymphoma cell line that lacks the characteristic chromosome translocation leading to constitutive c-myc activation. We analyzed LMP1-expressing and LMP1-suppressed BJAB cells as well as parental BJAB cells not harboring the LMP1 oncogene over 21 days for formation of multinucleated cells, 3D telomere dynamics, and the expression of key proteins of the shelterin complex at the transcriptional, translational, and topographic protein level. The results show that the chromosome ends (ie, the telomeres within the shelterin complex) are responsive to the expression of the LMP1 oncogene and that constitutive expression of the TRF2 protein protects cells against LMP1-induced multinucleation.

Figure 1. Schematic representation of the tet-Off system. The tTA binds specifically to the tet-Off (tetO) operator sequences upstream of the CMV promoter (P_{CMV}). The tetO/P_{CMV} represents the tetracycline response element (TRE). In the presence of tetracycline, the binding of this antibiotic to tTA blocks its binding to the TRE (left), and transactivation of the LMP1 oncogene does not occur. The LMP1 oncogene, under the control of TRE, is activated by tTA (right) in the absence of tetracycline resulting in LMP1 oncoprotein expression. tetR, tetracycline repressor protein; VP16, herpes-simplex virus encoded transcriptional activator.

Material and methods

Cell lines

Cells were grown in bicarbonate-buffered RPMI-1640 medium supplemented with 10% fetal calf serum, penicillin (200 U/mL), and streptomycin (200 mg/mL) and were incubated at 37°C in a humidified atmosphere containing 5% CO_2.

The stable BJAB transfectants used have been described in detail previously.[22] BJAB-tTA is a stable transfectant constitutively expressing a tetracycline-regulated transactivator (tTA) from a cytomegalovirus-immediate early promoter on the plasmid pJEF-3. BJAB-tTA-LMP1 is a dual stable transfectant (plasmid pJEF-3 and LMP1-bearing plasmid pJEF-6) expressing LMP1 from the plasmid pJEF-6 upon activation of its promoter by tTA in the absence of tetracycline (Figure 1). The tTA was inhibited by incubating cells with tetracycline (1 μg/mL) and activated after washing cells in tetracycline-free medium with subsequent incubation in tetracycline-free medium. Hence, BJAB-tTA and BJAB-tTA-LMP1 with and without tetracycline (1 μg/mL) were cultured and analyzed at distinct time points for LMP1 expression and multinuclearity, nuclear volumes, and 3D telomere organization as well as TRF1, TRF2, and POT1 topography in interphase nuclei.

Percentage of multinucleated cells

The percentage of multinucleated cells was determined as follows: on days 1, 7, 14, and 21 of the experiments, 200 cells (as described in the legend for Figure 2) were counted on cytocentrifuge slides by 3 independent researchers on 5 independent triplicate experiments.

For the pIRESPuro3_mycTRF2 expression experiments, the evaluation of the percentage of multinucleated cells was performed with the Operetta system (PerkinElmer, Woodbridge, ON, Canada). More than 300 cells were counted by imaging on Operetta during the course of the experiment (10 days) in 3 independent experiments. Briefly, about 100 000 cells for each sample were colored in 200 μL RPMI-1640 10% fetal bovine serum containing 1 μg/mL H33342 and 0.1 μg/mL calcein AM for 30 minutes at 37°C. Cells were centrifuged in optical 96-well plates at 800 rpm for 5 minutes before acquisition on Operetta. About 20 fields at ×100 magnification were acquired on Operetta, with multiple imaging along the z-axis by using 4,6 diamidino-2-phenylindole (DAPI) and green fluorescent protein filters for H33342
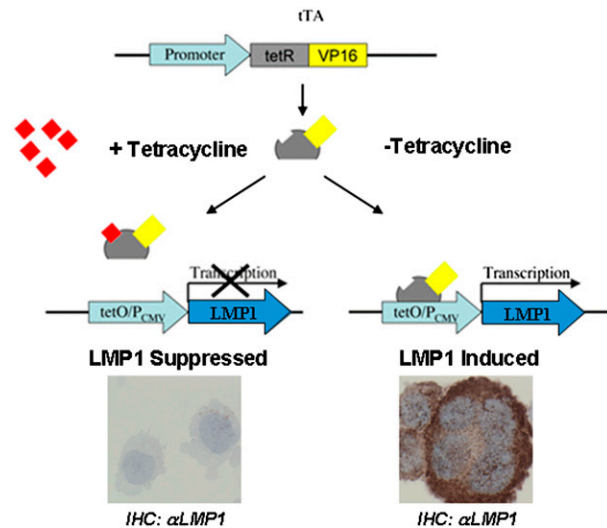
and calcein AM, respectively. Images of each field were manually observed to count nuclei (H33342) per live cell (calcein AM).

LMP1 mmunohistochemistry

Immunohistochemistry was performed as described[23] on 3D fixed cells[8] by using murine monoclonal CS.1-4 anti-LMP1 antibodies (Dako) as primary antibodies at a dilution of 1:200. The secondary antibody was a goat anti-mouse antibody coupled to peroxidase at a dilution of 1:1000. Nuclei were counterstained with DAPI. Analysis was performed by using a Zeiss AxioImager Z1 microscope (Zeiss, Toronto, Canada). Images were acquired with a cooled AxioCam HR black-and-white (B&W) camera (Zeiss).

Immunofluorescence

Immunofluorescence was performed on cytocentrifuged cells. Briefly, cells were fixed on slides with 3.7% paraformaldehyde in phosphate-buffered saline (PBS). Fixed cells were then permeabilized with 0.1% Triton X-100 in PBS and blocked with 0.1% Triton X-100, 0.5 μg/mL bovine serum albumin in PBS. LMP1 was revealed by using the primary mouse LMP1 antibody (sc-57721; Santa Cruz Biotechnology) at a dilution of 1:150 and with a secondary anti-mouse antibody coupled to fluorescein isothiocyanate at a dilution of 1:200. TRF2 was revealed by rabbit polyclonal antibodies against TRF2 (Santa Cruz Biotechnology) at a dilution of 1:100. The secondary antibody was mouse anti-rabbit immunoglobulin G fluorescein isothiocyanate at a dilution of 1:1000. Nuclei were counterstained with Hoechst H33342. Analysis was performed by using a Zeiss AxioImager Z1 microscope (Zeiss). Images were acquired with a cooled AxioCam HR B&W camera (Zeiss).

Western blotting

Whole cell extracts were prepared by lysing cells in Laemmli sample buffer (1×; 10% glycerol, 5% b-mercaptoethanol, 2.3% sodium dodecyl sulfate, 62.5 mM tris[hydroxymethyl]aminomethane-HCl [pH 6.8], and 0.1% bromophenol blue). Equal amounts of total protein were loaded into each well of 10% sodium dodecyl sulfate polyacrylamide gel electrophoresis and transferred to nitrocellulose membranes. Protein amounts were revealed with primary antibodies against LMP1 (sc-57721; Santa Cruz Biotechnology), TRF1 (provided by Titia De Lange), TRF2 (IMG-124A; Imgenex), POT1 (custom synthesis at Sigma-Genosys and affinity purified), α-tubulin

Figure 2. LMP1 expression in BJAB-tTA-LMP1 Burkitt lymphoma cells is associated with multinuclearity. Original magnification ×640, Zeiss AxioImager Z1 microscope. (A) LMP1-suppressed transfectants at day 7 still reveal uniform Burkitt cell morphology with only a few binucleated or large mononuclear cells (arrows) (Pappenheim staining). (B) Immunostaining with anti-LMP1 monoclonal antibody CS.1-4 confirms successful LMP1 suppression through tetracycline. (C) LMP1-expressing transfectants at day 7 contain multiple RS-like giant cells. Arrow points to a satellite nucleus (Pappenheim staining). (D) Strong LMP1 expression is confirmed with anti-LMP1 monoclonal antibody CS.1-4. (E) LMP1 induced accumulation of multinuclear cells. BJAB-tTA-LMP1 cells were induced for the expression of LMP1 for 21 days by removal of tetracycline. Samples from LMP1-induced and LMP1-suppressed cells at days 1, 7, 14, and 21 were cytocentrifuged and counted for the presence of multinucleated cells. For each time point, 200 cells were counted in 15 independent experiments. LMP1-induced formation of RS-like giant cells is evident. *$P < .05$; **$P < .0001$.
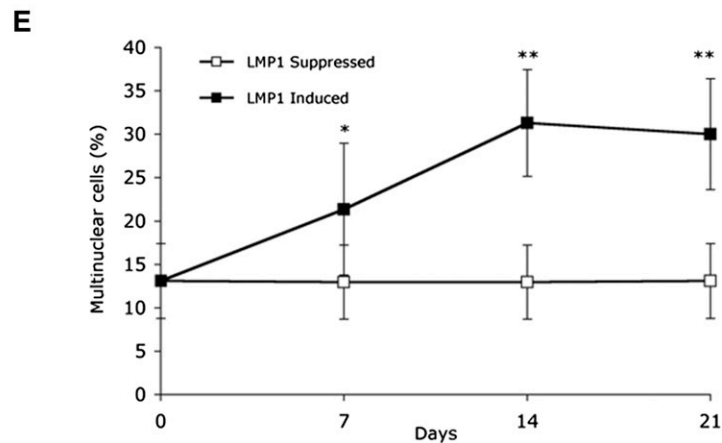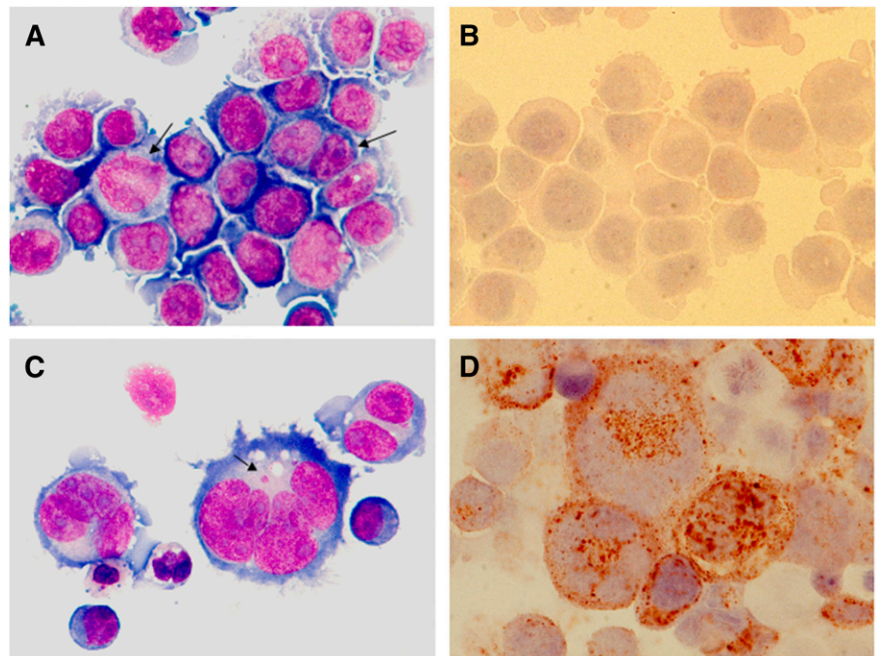
(ab4074; AbCam), and *ACTB* (A2066; Sigma) and by using peroxidase-conjugated secondary antibodies with enhanced chemiluminescence detection reagent (Amersham) on radiograph film.

Quantitative reverse-transcription polymerase chain reaction

The levels of messenger RNA (mRNA) expression for LMP1 and shelterin proteins TRF1, TRF2, POT1, and TPP1 were analyzed by quantitative reverse-transcription polymerase chain reaction. About 300 ng of total RNA (Trizol purified) from BJAB-tTA-LMP1 was reverse transcribed by using Maloney murine leukemia virus reverse transcriptase and random hexamer. One-fiftieth of the reverse transcriptase reaction was then used for each SYBR Green–based real-time polymerase chain reaction using specific primers for each gene. The levels of targeted mRNA are normalized with *ACTB*, glyceraldehyde-3-phosphate dehydrogenase (GAPDH), and β2-microglobulin expression.

    Primers for our experiments were designed according to Rozen et al,[24] if not otherwise specified: 5′-TGCACCACCAACTGCTTAGC-3′ and 5′-GGCATGGACTGTGGTCATGAG-3′ for GAPDH, 5′-GCGGGAAATC GTGCGTGACATT-3′ and 5′-GATGGAGTTGAAGGTAGTTTCGTG-3′ for *ACTB*, 5′ATGTCTCGCTCCGTGGCCTTA-3′ and 5′-ATCTTGGGC TGTGACAAAGTC-3′ for β2-microglobulin, 5′-CAACCAATAGAGTC CACCAGT-3′ and 5′-TCTTCAGAAGAGACCTTCTCT-3′ for LMP1,[25]

5′-GCTGTTTGTATGGAAAATGGC-3′ and 5′-CCGCTGCCTTCATTA GAAAG-3′ for TRF1,[26] 5′-GTACCCAAAGGCAAGTGGAA-3′ and 5′-TGACCCACTCGCTTTCTTCT-3′ for TRF2, and 5′-TGAAGTTCTTTA AGCCCCCA-3′ and 5′-AGCCTGTGAAAGCGAACAAT-3′ for POT1.

Plasmid pIRESPuro3_mycTRF2

The expression plasmid pIRESPuro3_mycTRF2, which carries the human TRF2 with an myc tag in the N-terminal region of the protein was produced by transferring a blunted *Hin*dIII-*Eco*RI fragment from pLPC-NMYC TRF2 (Addgene plasmid 16066)[27] into the pIRESPuro3 vector (Clontech) cleaved with *Eco*RV and *Eco*RI. This plasmid allows the expression of two open reading frames from the same bicistronic transcript and selection of a population of cells resistant to puromycin and expressing the myc-tagged version of TRF2.

Plasmid electroporation and establishment of BJAB-tTA-LMP1/ mycTRF2 cells. The pIRESPuro3_mycTRF2 plasmids were introduced into BJAB-tTA-LMP1 cells by electroporation as follows: 2×10^6 cells were washed twice with serum-free RPMI-1640 and resuspended in 200 μL of ice-cold potassium-PBS containing 10 μg of plasmid DNA. Electroporation was performed in a 4-mm-gap cuvette with the gene Pulser at 250V and 950 μF. To select a population of stable transfectants, cells were transferred to a culture dish and allowed to recover from electroporation in media without the selective agent. Puromycin was introduced at 0.3 μg/mL 48 hours after

electroporation, and selective media was changed every 4 days until survival of the population.

Telomere qFISH

BJAB-tTA and BJAB-tTA-LMP1 cells were collected (200*g* for 10 minutes), resuspended in PBS containing 3.7% formaldehyde (Fluka), and incubated for 20 minutes. Thereafter, the telomere qFISH protocol was performed[7,28] by using a Cy3-labeled peptide nucleic acid probe (Dako). After telomere qFISH was performed, interphases were imaged by using a Zeiss AxioImager Z1 microscope with a cooled AxioCam HR B&W camera, DAPI, and Cy3 filters in combination with a Planapo 63×/1.4 oil objective lens. Images were acquired by using Axiovision 4.6 software (Zeiss) in multichannel mode followed by constraint iterative deconvolution as specified below.

3D image acquisition

At least 30 mononucleated cell interphase nuclei and at least 30 RS-cell–like interphase polykaria were analyzed for both cell lines. Axiovision 4.6 software with a deconvolution module and a rendering module was used. For every fluorochrome, the 3D image consisted of a stack of 80 images with a sampling distance of 200 nm along the z-axis and 107 nm in the x- and y-axis directions. The constrained iterative algorithm option was used for deconvolution.[29]

3D image analysis for telomeres

Telomere measurements were done with the TeloView 3D image analysis program.[30] By choosing a simple threshold for the telomeres, a binary image was found. Based on that, the center of gravity of intensities was calculated for every object resulting in a set of coordinates (x, y, z) denoted by crosses on the screen. The integrated intensity of each telomere was calculated because it was proportional to the telomere length.[30]

Telomere aggregates

Telomere aggregates are defined as clusters of telomeres that are found in close association and cannot be further resolved as separate entities at an optical resolution limit of 200 nm.[31]

Telomere length

Telomeres with a relative fluorescent intensity (x-axis) ranging from 0 to 5000 units were classified as very short, intensity from 5000 to 15 000 units defined as short, intensity from 15 000 to 30 000 units as mid-sized, and intensity >30 000 units as large.[9]

Telomere volume

Total telomere volume is the sum of all very short, short, mid-sized, and large telomeres and aggregates within one mononuclear or multinucleated cell.

Nuclear volume

The nuclear volume was calculated according to the 3D nuclear DAPI staining as described earlier.[32]

Spectral karyotyping

Spectral karyotyping (SKY) was performed by using the SKY kit for human chromosomes (ASI, Vista, CA) and following the manufacturer's protocol. Slides were imaged by using an Axioplan 2 microscope with a 63×/1.4 oil objective (Zeiss) and were analyzed by using Case Data Manager 4.0 software (ASI, Vista, CA). Twenty metaphases were imaged and analyzed for both cell lines. Rearrangements were scored and statistically analyzed.

Statistical analysis

For both cell lines, normally distributed parameters are compared between the two types of cells using nested or two-way analysis of variance. Then multiple comparisons using the least-square means tests were performed in which interaction effects between two factors were found to be significant. Other

Table 1. 3D telomere characteristics in RS-like cells without LMP1 (BJAB-tTA-LMP1 with tetracycline; n = 104) and with LMP1 (BJAB-tTA-LMP1 without tetracycline; n = 96)

Analysis/parameter for pool of days 7, 10, and 21	LMP1 suppressed	LMP1 induced	*P*
Total nuclear volume (μm^3)	2958 ± 1891	5375 ± 3572	<.0001
No. of telomeres per cell	98.9 ± 41.7	149.1 ± 71.6	<.0001
No. of telomeres per 1000 μm^3 of nuclear volume	38.1 ± 14.3	32.2 ± 16.4	.0070
% of short telomeres (<15 000 units)	76.9	77.1	>.05*
No. of telomere aggregates per cell	11.8 ± 6.1	18.0 ± 10.1	<.0001
% of cells with ≥20 aggregates	9.9	38.5	<.0001

Values are means ± standard deviation unless otherwise noted.
*Not significant.

parameters that were not normally distributed were compared by using a nonparametric Wilcoxon rank sum test. Significance levels were set at $P = .05$. Analyses were performed by using SAS v9.1 programs unless otherwise specified.

Results

Constitutive LMP1 expression induces multinuclearity

To assess the inducible system for expression of LMP1 (Figure 1), BJAB-tTA-LMP1 cells were cultured in either the presence or absence of tetracycline, and LMP1 expression was determined by immunocytochemistry (Figure 2). In the presence of tetracycline, LMP1 expression remained below detectable levels (Figure 2A-B), whereas in its absence, the LMP1 oncoprotein was expressed in more than 90% of cells at days 7, 14, and 21 (Figure 2C-D). Most importantly, LMP1 expression was associated with multinuclearity, and many of the cells resembled RS cells. The fraction of multinuclear giant cells increased from a baseline level of about 13% at day 1 to 21% at day 7 and to about 30% to 35% at day 14, remaining at that level up to day 21 (Figure 2E). In BJAB-tTA-LMP1 suppressed cells (with tetracycline), a baseline level of multinuclear cells of about 13% was observed at each time point. A comparable stable baseline level of multinuclear cells was also observed in the parental BJAB-tTA cells with and without tetracycline (results not shown).

Constitutive LMP1 expression changes the 3D nuclear telomere organization

Constitutive LMP1 expression over time led to a highly significant increase in nuclear volume and telomere aggregates but a decrease of the total number of telomeres per 1000 μm^3 of nuclear volume (calculated after DAPI staining) when comparing the LMP1-positive multinucleated cells with LMP1-negative, mainly binucleated cells (Table 1). When the 3D telomere dynamics in the LMP1-induced multinucleated cells was analyzed, a clear difference was observed in the telomere amount and length distribution compared with mononucleated cells (Figure 3). The 3D telomere dynamics analysis in LMP1-repressed RS-like cells revealed an increase in the amount of small telomeres but less than what was observed for the LMP1-induced RS-like cells, suggesting a common way for multinucleation in both contexts (LMP1-repressed and LMP1-induced). However, changes of the 3D telomere dynamics became much more pronounced over time in LMP1-induced cells in terms of telomere changes and multinucleation level (supplemental Figure 1, available on the *Blood* Web site). After 2 to 3 weeks of constitutive LMP1

Figure 3. 3D telomere dynamics of multinucleated RS-like cells in the Burkitt lymphoma cell line BJAB-tTA-LMP1. Telomere distribution according to size. Results are based on 3D analysis of 30 cells for each time point. Frequency (y-axis) and relative fluorescent intensity (ie, size of telomeres) (x-axis) reveal individual telomere profiles for each time point. Telomeres with a relative fluorescent intensity (x-axis) ranging from 0 to 5000 units are classified as very short, intensity from 5000 to 15 000 units as short, intensity from 15 000 to 30 000 units as mid-sized, and intensity >30 000 units as large. LMP1 expression induces multinucleated RS-like cells with abundant very short and short telomeres when compared with mononuclear cells at day 21.
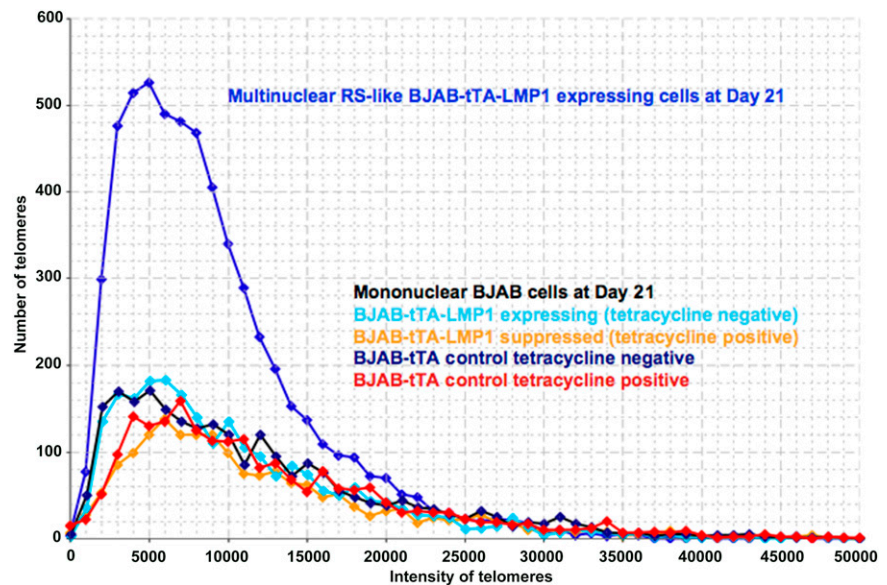
expression and several rounds of endomitosis, the multinuclear LMP1-expressing BJAB-tTA-LMP1 RS-like cells contained mainly very short telomeres; telomere-poor ghost nuclei and also telomere overloaded, aggregate-rich satellite nuclei could be identified (Figure 4 and supplemental Figure 2). Thus LMP1 is a powerful modulator of 3D nuclear telomere dynamics associated with formation of multinuclear BJAB cells ($P < .0001$).

SKY confirms generation of LMP1-induced outré giant cells and chromosome-poor ghost cells

Twenty metaphase preparations of BJAB-tTA-LMP1–expressing cells (tetracycline negative) were analyzed at days 1 and 14, and 20 metaphase preparations of BJAB-tTA-LMP1–suppressed cells (tetracycline positive) were analyzed at day 14 for overall chromosomal changes by using SKY. The images were analyzed by using Case Data Manager and SKY View software. Every metaphase analyzed had some form of chromosomal rearrangement. Conclusive analyses were possible in 15 of 20 metaphases at day 1, and in 18 of 20 metaphases at day 14 for LMP1-expressing metaphases, and in 14 of 20 LMP1-suppressed metaphases. Constitutive LMP1 expression at day 14 was associated with highly polyploid giant cells with up to 316 chromosomes (supplemental Figure 3). Yet severely hypoploid ghost cells (19 and 29 chromosomes) were also observed (supplemental Table 1).

Constitutive LMP1 expression suppresses shelterin proteins and promotes changes in their topographical distribution

Changes in telomeric 3D dynamics and formation of aggregates suggest a perturbation of telomere protection that is governed by proteins of the shelterin complex. Analysis of the transcriptional expression level of key shelterin genes reveals a rapid decrease in the level of TRF2 mRNA after induction of LMP1. At only 1 day after LMP1 induction, the level of TRF2 had decreased to 50% of that found in parallel LMP1-suppressed cells. TRF1 and POT1 also appear to be downregulated but to a lesser extent (Figure 5A). Moreover, this suppression was reversible upon delayed withdrawal of LMP1 suppression (ie, suppression at day 3 reflects cells that have been induced up to day 3 and suppressed for LMP1 expression from day 3 onward). The levels of shelterin proteins TRF2 and POT1

correlate with the shelterin mRNA levels observed (Figure 5B). This tight regulation of shelterin genes through LMP1 expression suggests that LMP1 has a major impact on shelterin protein expression, mostly on TRF2, and that it occurs at LMP1 oncoprotein levels similar to those observed in lymphoblastoid cell lines (supplemental Figure 4). Combined FISH-TRF2 immunostaining confirmed the disappearance of telomere-associated TRF2 spots, consistent with the formation of abundant small TRF2 free telomeres in the RS-like cells (Figure 5C). Analogous findings are confirmed by combined 3D telomere FISH-TRF2 immunohistochemistry on primary H and RS cells (supplemental Figure 5).

Constitutive myc-tagged TRF2 expression compensates LMP1-induced endogenous TRF2 suppression and blocks multinucleation

The previous sections suggest that LMP1 induced a strong reduction of the transcription and translation of the endogenous TRF2 gene (Figure 5A-B). Previously, it had been shown that an absence or reduction of TRF2 proteins on telomeres results in nonhomologous end joining (NHEJ) of telomeres with formation of giant chromosomes[33] remarkably similar to those observed in RS cells.[21] We therefore hypothesized that LMP1-induced TRF2 suppression could be a major factor in formation of multinucleated cells via an induction of telomere-led genome instability. If that was the case, overriding LMP1-dependent TRF2 suppression by CMV-driven myc-TRF2 expression should block NHEJ and multinucleation induced by LMP1. Indeed, in the double stable transfectant BJAB-tTA-LMP1/mycTRF2, the constitutive myc-TRF2 expression is not influenced by LMP1 and suppresses LMP1 associated multinucleation (Figure 6). Thus, induction of multinucleation by LMP1 in an experimental post germinal center B-cell system is correlated with the expression level of shelterin protein TRF2.

Discussion

Our in vitro results using an experimental, germinal center–derived B-cell system with inducible LMP1 expression reveal novel
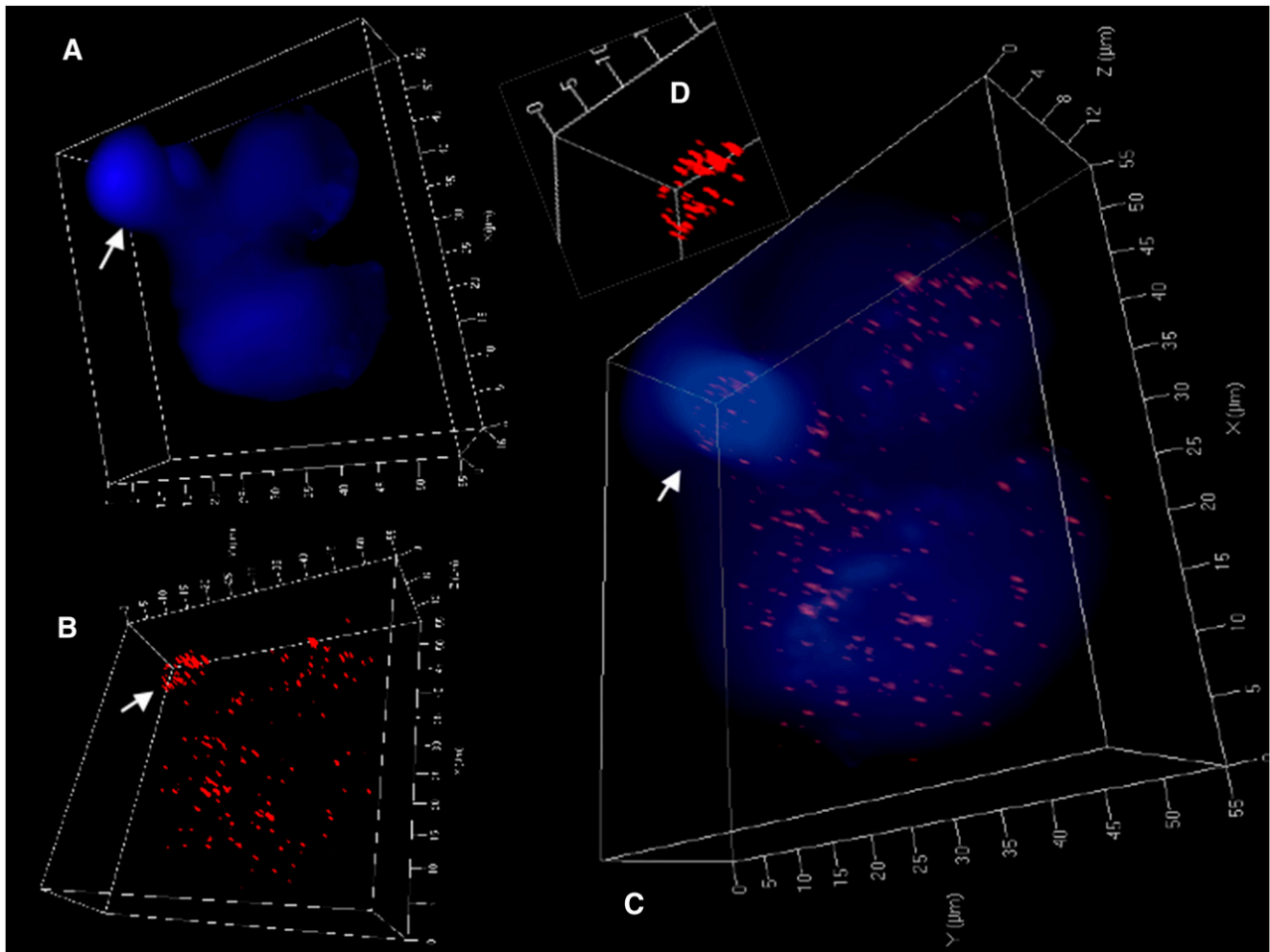
Figure 4. 3D identification of disturbed nuclear telomere organization in a trinuclear LMP1-expressing RS-like BJAB-tTA-LMP1 cell. (A) 3D reconstruction of nuclear DNA (DAPI; blue) in surface mode reveals a small folded satellite nucleus (arrow), a second nucleus at the upper right and a third large nucleus at the bottom. (B) 3D telomere (red) reconstruction in surface mode reveals abundant telomeres in lower part of the small satellite nucleus (arrow) and irregular telomere distribution in the large nucleus. (C) Combined 3D nuclear staining confirms telomere rich DNA dense satellite nucleus (arrow) and uneven telomere distribution in the large nucleus. (D) Inset (folded satellite nucleus) localizes short telomeres and also aggregates to its lower part. Further 3D telomere analysis of this satellite nucleus is shown in supplemental Figure 2B.

functions and targets of this oncoprotein. Induced expression of LMP1 exerts profound effects on the expression levels of key telomeric proteins such as TRF1, TRF2, and POT1 (Figure 5). In particular, LMP1-induced TRF2 downregulation appears to be a major factor in the formation of giant chromosomes and multinucleated cells through endomitosis and/or endoreplication (Figure 6 and supplemental Figure 3). Furthermore, TRF2 localization as well as the 3D nuclear telomere organization associated with the formation of RS-cell–like multinucleated cells appears to be profoundly changed.

Analogous changes during the transition from H cells to RS cells have been reported in HL cell lines and diagnostic lymph node biopsies of classical EBV-negative and EBV-positive HL.[8,9] Thus, the LMP1-inducible germinal center–derived BJAB-Burkitt cell line offers an excellent platform for studying the molecular impact of constitutive LMP1 expression in a germinal center–derived B-cell setting like that encountered in EBV-associated HL.

According to Thorley-Lawson and Gross,[34] the H and RS cells of EBV-associated HL arise from EBV-infected germinal center B cells, which constitutively express LMP1 at low levels. These lymphocytes have a $CD10^+CD38^+AID^+bcl-6^+$ phenotype and reside at a very low frequency (1 to 2/10^5) within the germinal centers of tonsils of EBV-positive adolescents.[35] Indeed, the risk

of developing EBV-associated HL after symptomatic infectious mononucleosis is increased fourfold within 4 years after the event,[16] and relevant differences in EBV association are observed according to socioeconomic status,[15] patient age, and geographic localization.[36] The incidence of EBV-associated HL is <30% in an unselected Swedish population,[37] whereas it is about 70% in Kenyan adults and even up to 100% in Kenyan infants[38] suggesting a pathogenetic implication of the virus in EBV-associated HL.

Ex vivo EBV infection of human B lymphocytes results, after 2 weeks, in nonclonal structural chromosome aberrations such as dicentric chromosomes and unbalanced translocations without telomere shortening but with partial displacement of TRF2 from the telomeres,[19] and EBNA1 promotes telomere dysfunction via induction of oxidative stress.[20] SKY of HL cell lines identifies complex chromosomal rearrangements already in H cells that progress through multiple BBF cycles to end-stage multinuclear RS cells.[21] In these RS cells, γ-H2AX, Mre11, and Rad51c are upregulated and TRF2 is mainly cytoplasmic.[8] This is consistent with telomere dysfunction because conditional TRF2 deletion elicits an ataxia-telangectasia-Rad3 (ATM)–mediated telomere damage response with γ-H2AX upregulation resulting in telomere fusions and consequently giant chromosomes in mouse fibroblasts[39] as well as in endoreplication and giant hepatocytes.[33,40] Moreover, conditional
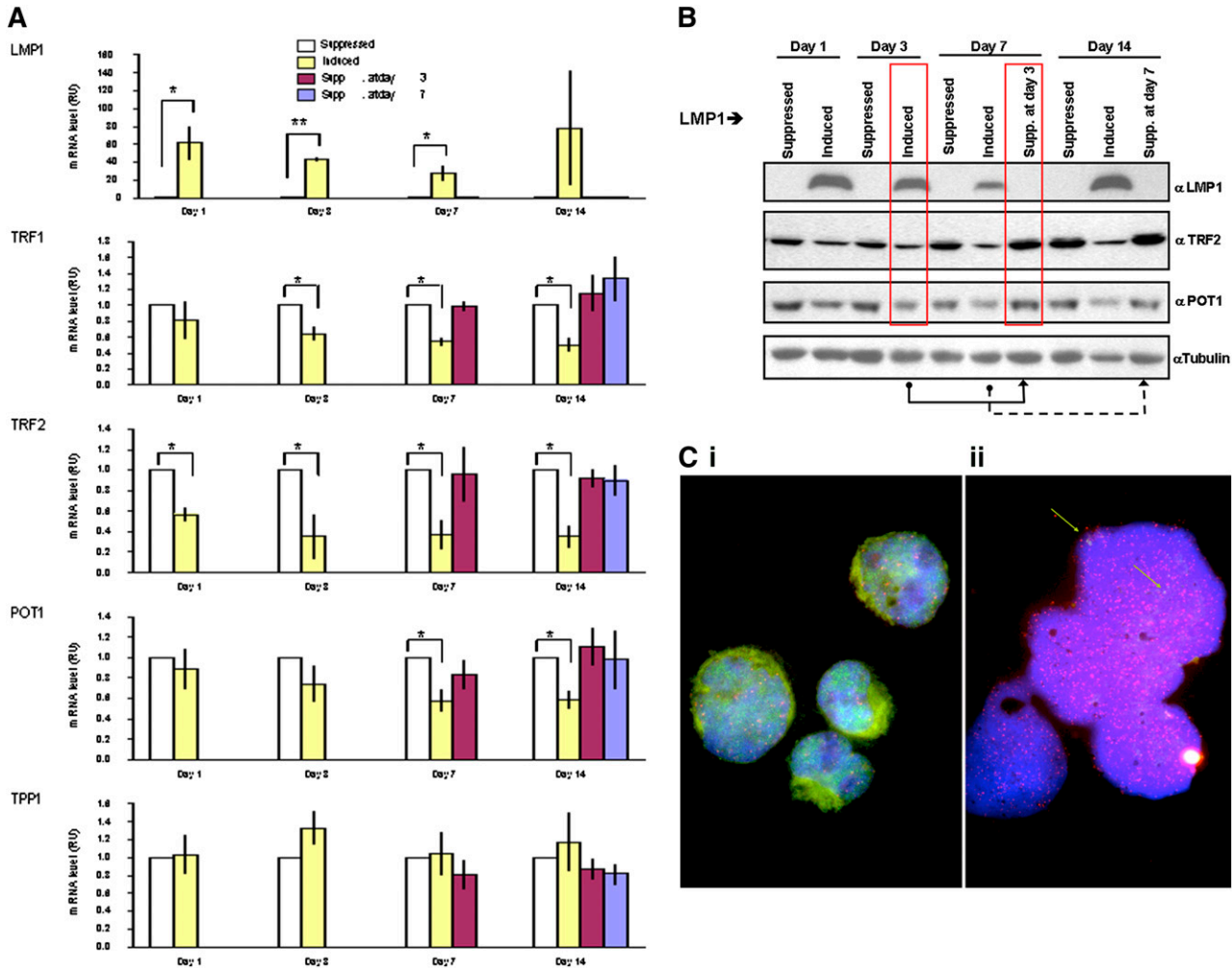
Figure 5. LMP1-induced changes in expression levels of shelterin RNAs and proteins are reversible. (A) Quantitative reverse-transcriptase polymerase chain reaction analysis of the mRNA expression of indicated shelterin genes on LMP1 expression and suppression. The mRNA levels of indicated genes (in relative units) at days 1, 3, 7, and 14 are normalized with expression of 3 housekeeping genes to the LMP1-suppressed cells at each time point. Also shown are levels for the mRNAs at days 7 and 14 if the expression of LMP1 was suppressed at day 3 (burgundy bars) or at day 14 if LMP1 expression was suppressed at day 7 (blue bars). Bars show mean values ± standard deviation of 3 independent experiments. *$P < .05$; **$P < .0001$ by Student t test. (B) LMP1 induced changes in expression levels of indicated shelterin proteins. Upper panel: BJAB-tTA-LMP1 cells were induced for the expression of LMP1 for 3, 7, and 14 days by removal of tetracycline. Protein levels of LMP1, TRF2, POT1, and α-tubulin as loading control were analyzed by western blotting by using corresponding antibodies. Reduction of shelterin proteins is observed (TRF2 and POT1) when LMP1 expression is induced. The suppression of LMP1 at day 3 returns shelterin proteins to the initial level of expression at day 7 (red boxes), and the suppression of LMP1 induction at day 7 returns shelterin proteins to the initial level of expression at day 14. Representative results from 3 independent experiments are shown. (C) Combined telomere FISH (red) and TRF2 immunostaining (green). Panel Ci: BJAB-tTA-LMP1–suppressed transfectant at day 14 shows nuclear TRF2 either free (green) or associated with mainly midsized telomeres (red) resulting in an orange-yellow signal in mononuclear cells. Panel Cii: BJAB-tTA-LMP1–induced cell with RS-like morphology. Abundant small telomeres and aggregates but nearly absent TRF2 (green arrows) were observed. Nuclei were counterstained with DAPI (blue).

deletion of TRF1 induces chromosomal fragility resulting in chromosome concatenation, sister chromatid fusions, and multitelomeric signals.[41-43] Conditional deletion of POT1 activates the ATM-related DNA damage response[33,44] allowing to bypass mitosis and to generate tetraploidy.[45] Analogous results associated with downregulation of shelterin proteins are observed in this study. However, and most importantly, the observations reported here concern the setting of stable LMP1 oncoprotein expression in post germinal center B cells, which is a hallmark of H and RS cells in EBV-associated HL.

The results show that LMP1 exerts profound effects on the shelterin proteins TRF1, TRF2, and POT1. Continuous LMP1 expression results in their substantial downregulation at the transcriptional and translational level and is associated with a highly significant formation of multinucleated RS-like cells ($P < .0001$). This downregulation is completely reversible upon cessation of LMP1 oncoprotein expression,

underscoring a tight interference with the endogenous shelterin protein expression. This effect is most pronounced for TRF2, whose expression is crucial in avoiding NHEJ recombination, which leads to giant chromosomes, hyperploidy, and endomitosis.[39,45] The data also show that compensation of the LMP1-induced downregulation of TRF2 by CMV-driven and thus LMP1-independent myc-tagged TRF2 expression successfully blocks formation of multinucleated RS-like cells (Figure 6B). We conclude that downregulation of TRF2 by expression of LMP1 induces multinuclearity. This finding largely explains earlier observations in which a transient expression of LMP1 in the EBV-negative Hodgkin cell lines L-428, KMH2, and HD-MyZ significantly increases the formation of RS cells.[46-48] Thus, LMP1 appears to mimic and/or accelerate signaling pathways identical to those involved in the pathogenesis of EBV-negative HL,[47] leading to the formation of short and very short telomeres without TRF2 protection as observed in EBV-negative HL (supplemental Figure 5).
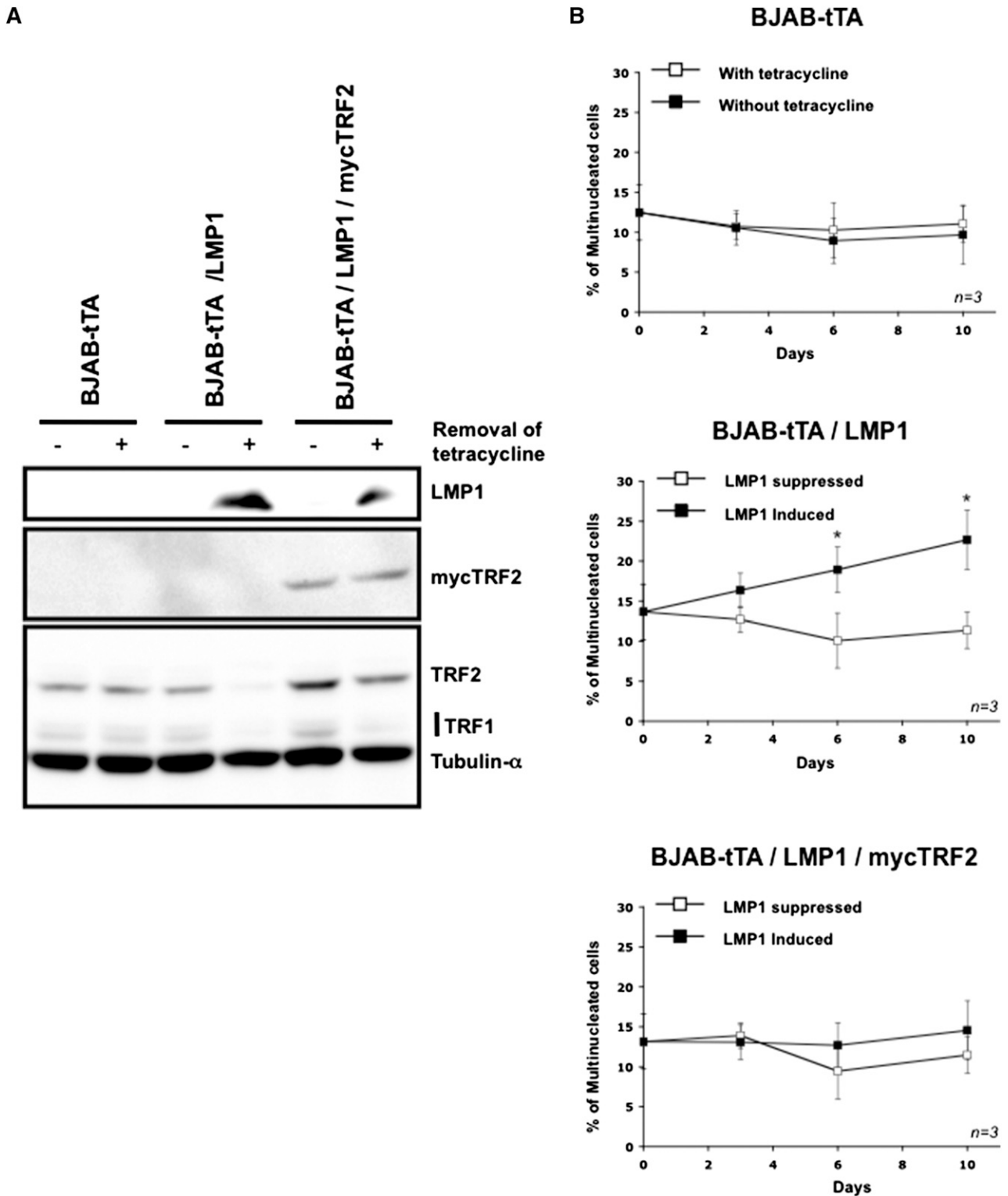
Figure 6. Maintenance on the expression of mycTRF2 after induction of LMP1 abolishes multinuclearity. (A) Representative western blot for the expression of mycTRF2, TRF2, and TRF1 in cells exposed for 3 days to the removal of tetracycline. Upper panel: LMP1 expression. Middle panel: expression of mycTRF2 revealed with anti-myc antibody. Lower panel: expression of TRF2 and TRF1 compared with α-tubulin as loading control, using a mix of antibody. In the double stable transfectant BJAB-tTA-LMP1/mycTRF2 (lanes 5 and 6) mycTRF2 is equally expressed independent of LMP1 expression, whereas total TRF2 (LMP1-dependent TRF2 and mycTRF2) is high in the presence of tetracycline (LMP1 suppressed, lane 5) but equal to mycTRF2 in the absence of tetracycline (LMP1 expressed, lane 6). Note also the LMP1-induced suppression of TRF1 (lanes 4 and 6). (B) Count of multinucleated cells by using the Operetta system in the presence or absence of tetracycline over a period of 10 days. Cell line analyzed is indicated in top of each panel. LMP1 expression results in a significant increase of bi- or multinuclear cells only in the BJAB-tTA-LMP1–induced cells (mid panel), whereas LMP1-independent, CMV-driven TRF2 expression compensates the LMP1-induced TRF2 suppression, abolishing multinucleation (bottom panel). Based on 3 independent experiments. *$P < .05$, Student t test).

The molecular events triggering the early steps of EBV-associated HL are largely unknown. Downregulation of CD99 (mic2) appears to be involved in this process,[49] and the mononuclear precursor H cells exhibit multiple random chromosomal rearrangements.[50,51] These complex chromosomal patterns are the result of ongoing BBF cycles as demonstrated by SKY combined with telomere FISH[21]; for example, a t(1;17) found in an H cell becomes a four-way translocation in an end-stage RS cell t(1;17;13;18) associated with interstitial telomere signals and telomere-free chromosome ends.[21] This dynamic process of nuclear remodeling probably begins in the few monoclonal circulating B cells[6] or even earlier in activated EBV-infected tonsillar germinal center B cells, which escape immuno-surveillance.[35] Substantial LMP1-induced alterations in the expression of several shelterin proteins, which act as gatekeepers for correct DNA replication and normally protect the chromosome ends[52,53] may substantially contribute to the unraveling of the molecular pathogenesis of EBV-associated HL.

The data presented in this article, in particular the LMP1-induced downregulation of TRF1, TRF2, and POT1 associated with multi-nucleation, as well the suppression of the LMP1 associated multi-nucleation through an LMP1-independent induced re-expression of TRF2, strongly support our recent hypothesis of EBV-associated HL as a shelterin-related disease.[54] Based on our results, TRF2 appears to be a major target of LMP1 but not the sole downstream effector of telomere dysfunction in this setting.

Authorship

Contribution: B.L., S.M., R.W., and H.K. conceived the study and established its initial design; V.L., B.L., B.S., Z.L., S.M., and H.K. carried out experimental work; V.L., B.L., D.L., and H.K. performed experimental data analysis; H.K. prepared and finalized the manuscript; V.L., B.L., B.S., R.W., and S.M. performed critical revisions; and all authors read and approved the final manuscript.

Conflict-of-interest disclosure: The authors declare no competing financial interests.

Correspondence: Hans Knecht, Division of Hematology, Department of Medicine, Jewish General Hospital, 3755, Chemin de la Côte Ste-Catherine, McGill University, Montréal, QC, Canada H3T 1E2; e-mail: hknecht@jgh.mcgill.ca; Raymund J. Wellinger, Département de Microbiologie et Infectiologie, Faculté de Médecine et des Sciences de la Santé, Université de Sherbrooke, 3001, 12th Ave Nord, Sherbrooke, QC, Canada J1H 5N4; e-mail: raymund.wellinger@usherbrooke.ca; Sabine Mai, Manitoba Institute of Cell Biology, 675 McDermot Ave, Winnipeg, MB, Canada R3E 0V9; e-mail: sabine.mai@med.umanitoba.ca.

References

1. Hsu SM, Zhao X, Chakraborty S, et al. Reed-Sternberg cells in Hodgkin's cell lines HDLM, L-428, and KM-H2 are not actively replicating: lack of bromodeoxyuridine uptake by multinuclear cells in culture. Blood. 1988;71(5):1382-1389.

2. Newcom SR, Kadin ME, Phillips C. L-428 Reed-Sternberg cells and mononuclear Hodgkin's cells arise from a single cloned mononuclear cell. Int J Cell Cloning. 1988;6(6):417-431.

3. Kapp U, Yeh WC, Patterson B, et al. Interleukin 13 is secreted by and stimulates the growth of Hodgkin and Reed-Sternberg cells. J Exp Med. 1999;189(12):1939-1946.

4. Khan G. Epstein-Barr virus, cytokines, and inflammation: a cocktail for the pathogenesis of Hodgkin's lymphoma? Exp Hematol. 2006;34(4):399-406.

5. Küppers R. The biology of Hodgkin's lymphoma. Nat Rev Cancer. 2009;9(1):15-27.

6. Jones RJ, Gocke CD, Kasamon YL, et al. Circulating clonotypic B cells in classic Hodgkin lymphoma. Blood. 2009;113(23):5920-5926.

7. Louis SF, Vermolen BJ, Garini Y, et al. c-Myc induces chromosomal rearrangements through telomere and chromosome remodeling in the interphase nucleus. Proc Natl Acad Sci USA. 2005;102(27):9613-9618.

8. Knecht H, Sawan B, Lichtensztejn D, Lemieux B, Wellinger RJ, Mai S. The 3D nuclear organization of telomeres marks the transition from Hodgkin to Reed-Sternberg cells. Leukemia. 2009;23(3):565-573.

9. Knecht H, Sawan B, Lichtensztejn Z, Lichtensztejn D, Mai S. 3D Telomere FISH defines LMP1-expressing Reed-Sternberg cells as end-stage cells with telomere-poor 'ghost' nuclei and very short telomeres. Lab Invest. 2010;90(4):611-619.

10. Pallesen G, Hamilton-Dutoit SJ, Rowe M, Young LS. Expression of Epstein-Barr virus latent gene products in tumour cells of Hodgkin's disease. Lancet. 1991;337(8737):320-322.

11. Knecht H, Bachmann E, Brousset P, et al. Deletions within the LMP1 oncogene of Epstein-Barr virus are clustered in Hodgkin's disease and identical to those observed in nasopharyngeal carcinoma. Blood. 1993;82(10):2937-2942.

12. Murray PG, Billingham LJ, Hassan HT, et al. Effect of Epstein-Barr virus infection on response to chemotherapy and survival in Hodgkin's disease. Blood. 1999;94(2):442-447.

13. Claviez A, Tiemann M, Lüders H, et al. Impact of latent Epstein-Barr virus infection on outcome in children and adolescents with Hodgkin's lymphoma. J Clin Oncol. 2005;23(18):4048-4056.

14. Keegan TH, Glaser SL, Clarke CA, et al. Epstein-Barr virus as a marker of survival after Hodgkin's lymphoma: a population-based study. J Clin Oncol. 2005;23(30):7604-7613.

15. Dinand V, Arya LS. Epidemiology of childhood Hodgkins disease: is it different in developing countries? Indian Pediatr. 2006;43(2):141-147.

16. Hjalgrim H, Askling J, Rostgaard K, et al. Characteristics of Hodgkin's lymphoma after infectious mononucleosis. N Engl J Med. 2003; 349(14):1324-1332.

17. Louissaint A Jr, Ferry JA, Soupir CP, Hasserjian RP, Harris NL, Zukerberg LR. Infectious mononucleosis mimicking lymphoma: distinguishing morphological and immunophenotypic features. Mod Pathol. 2012;25(8):1149-1159.

18. Knecht H, Kongruttanachok N, Sawan B, et al. Three-Dimensional Telomere Signatures of Hodgkin- and Reed-Sternberg Cells at Diagnosis Identify Patients with Poor Response to Conventional Chemotherapy. Transl Oncol. 2012; 5(4):269-277.

19. Lacoste S, Wiechec E, Dos Santos Silva AG, et al. Chromosomal rearrangements after ex vivo Epstein-Barr virus (EBV) infection of human B cells. Oncogene. 2010;29(4):503-515.

20. Kamranvar SA, Masucci MG. The Epstein-Barr virus nuclear antigen-1 promotes telomere dysfunction via induction of oxidative stress. Leukemia. 2011;25(6):1017-1025.

21. Guffei A, Sarkar R, Klewes L, Righolt C, Knecht H, Mai S. Dynamic chromosomal rearrangements in Hodgkin's lymphoma are due to ongoing three-dimensional nuclear remodeling and breakage-bridge-fusion cycles. Haematologica. 2010; 95(12):2038-2046.

22. Floettmann JE, Ward K, Rickinson AB, Rowe M. Cytostatic effect of Epstein-Barr virus latent membrane protein-1 analyzed using

tetracycline-regulated expression in B cell lines. *Virology.* 1996;223(1):29-40.

23. Fukasawa K, Wiener F, Vande Woude GF, Mai S. Genomic instability and apoptosis are frequent in p53 deficient young mice. *Oncogene.* 1997; 15(11):1295-1302.

24. Rozen S, Skaletsky HJ. Primer3 on the WWW for general users and for biologist programmers. In: Krawetz S, Misener S, eds. Bioinformatics Methods and Protocols: Methods in Molecular Biology. Totowa, NJ: Humana Press; 2000: 365-386.

25. Ometto L, Menin C, Masiero S, et al. Molecular profile of Epstein-Barr virus in human immunodeficiency virus type 1-related lymphadenopathies and lymphomas. *Blood.* 1997;90(1):313-322.

26. Escoffier E, Rezza A, Roborel de Climens A, et al. A balanced transcription between telomerase and the telomeric DNA-binding proteins TRF1, TRF2 and Pot1 in resting, activated, HTLV-1-transformed and Tax-expressing human T lymphocytes. *Retrovirology.* 2005;2:77.

27. Smogorzewska A, de Lange T. Different telomere damage signaling pathways in human and mouse cells. *EMBO J.* 2002;21(16):4338-4348.

28. Chuang TC, Moshir S, Garini Y, et al. The three-dimensional organization of telomeres in the nucleus of mammalian cells. *BMC Biol.* 2004; 2:12.

29. Schaefer LH, Schuster D, Herz H. Generalized approach for accelerated maximum likelihood based image restoration applied to three-dimensional fluorescence microscopy. *J Microsc.* 2001;204(Pt 2):99-107.

30. Vermolen BJ, Garini Y, Mai S, et al. Characterizing the three-dimensional organization of telomeres. *Cytometry A.* 2005;67(2):144-150.

31. Mai S, Garini Y. The significance of telomeric aggregates in the interphase nuclei of tumor cells. *J Cell Biochem.* 2006;97(5):904-915.

32. Sarkar R, Guffei A, Vermolen BJ, Garini Y, Mai S. Alterations of centromere positions in nuclei of immortalized and malignant mouse lymphocytes. *Cytometry A.* 2007;71(6):386-392.

33. Denchi EL, de Lange T. Protection of telomeres through independent control of ATM and ATR by TRF2 and POT1. *Nature.* 2007;448(7157): 1068-1071.

34. Thorley-Lawson DA, Gross A. Persistence of the Epstein-Barr virus and the origins of associated lymphomas. *N Engl J Med.* 2004;350(13): 1328-1337.

35. Roughan JE, Thorley-Lawson DA. The intersection of Epstein-Barr virus with the germinal center. *J Virol.* 2009;83(8):3968-3976.

36. Glaser SL, Gulley ML, Clarke CA, et al. Racial/ethnic variation in EBV-positive classical Hodgkin lymphoma in California populations. *Int J Cancer.* 2008;123(7):1499-1507.

37. Enblad G, Sandvej K, Sundström C, Pallesen G, Glimelius B. Epstein-Barr virus distribution in Hodgkin's disease in an unselected Swedish population. *Acta Oncol.* 1999;38(4):425-429.

38. Weinreb M, Day PJ, Niggli F, et al. The consistent association between Epstein-Barr virus and Hodgkin's disease in children in Kenya. *Blood.* 1996;87(9):3828-3836.

39. Celli GB, de Lange T. DNA processing is not required for ATM-mediated telomere damage response after TRF2 deletion. *Nat Cell Biol.* 2005; 7(7):712-718.

40. Lazzerini Denchi E, Celli G, de Lange T. Hepatocytes with extensive telomere deprotection and fusion remain viable and regenerate liver mass through endoreduplication. *Genes Dev.* 2006;20(19):2648-2653.

41. Martínez P, Thanasoula M, Muñoz P, et al. Increased telomere fragility and fusions resulting from TRF1 deficiency lead to degenerative pathologies and increased cancer in mice. *Genes Dev.* 2009;23(17):2060-2075.

42. Okamoto K, Iwano T, Tachibana M, Shinkai Y. Distinct roles of TRF1 in the regulation of telomere structure and lengthening. *J Biol Chem.* 2008; 283(35):23981-23988.

43. Sfeir A, Kosiyatrakul ST, Hockemeyer D, et al. Mammalian telomeres resemble fragile sites and require TRF1 for efficient replication. *Cell.* 2009; 138(1):90-103.

44. He H, Wang Y, Guo X, et al. Pot1b deletion and telomerase haploinsufficiency in mice initiate an ATR-dependent DNA damage response and elicit phenotypes resembling dyskeratosis congenita. *Mol Cell Biol.* 2009;29(1):229-240.

45. Davoli T, Denchi EL, de Lange T. Persistent telomere damage induces bypass of mitosis and tetraploidy. *Cell.* 2010;141(1):81-93.

46. Knecht H, McQuain C, Martin J, et al. Expression of the LMP1 oncoprotein in the EBV negative Hodgkin's disease cell line L-428 is associated with Reed-Sternberg cell morphology. *Oncogene.* 1996;13(5):947-953.

47. Knecht H, Berger C, McQuain C, et al. Latent membrane protein 1 associated signaling pathways are important in tumor cells of Epstein-Barr virus negative Hodgkin's disease. *Oncogene.* 1999;18(50):7161-7167.

48. Chang KC, Chang Y, Jones D, Su IJ. Aberrant expression of cyclin a correlates with morphogenesis of reed-sternberg cells in Hodgkin lymphoma. *Am J Clin Pathol.* 2009;132(1):50-59.

49. Kim SH, Shin YK, Lee IS, et al. Viral latent membrane protein 1 (LMP-1)-induced CD99 down-regulation in B cells leads to the generation of cells with Hodgkin's and Reed-Sternberg phenotype. *Blood.* 2000;95(1):294-300.

50. MacLeod RA, Spitzer D, Bar-Am I, et al. Karyotypic dissection of Hodgkin's disease cell lines reveals ectopic subtelomeres and ribosomal DNA at sites of multiple jumping translocations and genomic amplification. *Leukemia.* 2000; 14(10):1803-1814.

51. Mader A, Brüderlein S, Wegener S, et al. U-HO1, a new cell line derived from a primary refractory classical Hodgkin lymphoma. *Cytogenet Genome Res.* 2007;119(3-4):204-210.

52. Wu Y, Zakian VA. Identity crisis when telomeres left unprotected. *J Mol Cell Biol.* 2010;2(1):14-16.

53. Londoño-Vallejo JA, Wellinger RJ. Telomeres and telomerase dance to the rhythm of the cell cycle. *Trends Biochem Sci.* 2012;37(9):391-399.

54. Knecht H, Righolt C, Mai S. Genomic instability: the driving force behind refractory/relapsing Hodgkin's lymphoma. *Cancers (Basel).* 2013;5(2): 714-725.